52nd IEEE Conference on Decision and Control
December 10-13, 2013. Florence, Italy

# On Real-Time Optimization of Airborne Wind Energy Generators

Aldo U. Zgraggen*, Lorenzo Fagiano, and Manfred Morari

*Abstract*— **Airborne wind energy generators aim to produce renewable energy by means of aerodynamic lift from tethered wings controlled to fly crosswind paths. The problem of optimizing the operation of such a generator in presence of limited information on wind speed and direction is considered, aiming to maximize the average power developed. First, a study of the traction force is presented for a general path parametrization. Then, the results of this analysis are exploited to design an algorithm to maximize the force, hence the power, in real-time. The algorithm uses only the measured traction force on the tether, and it is able to adapt the system's operation to maximize the average force with uncertain and time-varying wind. Numerical simulations are presented to highlight the effectiveness of the approach.**

## I. Introduction

Airborne wind energy (AWE) systems [1] aim to harness wind energy beyond the altitude of traditional wind mills, in stronger and more steady winds, using tethered wings. The tethers are used to transfer the energy down to the ground. Depending on the system layout, the energy is transferred to the ground as mechanical or electrical energy. To increase the power output, the wings are controlled to fly roughly perpendicular to the wind direction [2], in so-called crosswind paths. In the recent past, an increasing number of research groups started to develop new concepts of AWE systems, see e.g. [3], [4], [5], [6], [7], [8], [9], [10], [11], [12], [13], [14]. Automatic control of the tethered wings plays a major role for the efficiency and thus also economics of such energy generators. The goal is to control the wing in order to fly a crosswind path under state and input constraints, while maximizing the generated power. In order to maximize the power output, the wing should fly on a path that yields the highest traction force for the given wind condition. This problem has been studied by several research groups, see [11], [15], [16], [17], [18]. Most of these approaches employ an optimal path and a trajectory-following controller. Yet, the offline generated optimal trajectories are subject to model-plant mismatch, hence they may be sub-optimal or even infeasible in practice. Moreover, the mentioned approaches assume that the wind speed and direction at the wing's location are known in order to employ the computed optimal path. However, the wind field changes over distance and time and it is difficult to estimate with only a few measurement points, like those available with ground anemometers.

In order to tackle these issues, in this paper we propose a model-free optimization approach, based on real-time adaptation of the flown paths, with no exact knowledge of the wind conditions. At first, we analyze the influence of the crosswind path on the traction force, in order to asses the most important aspects of the flown trajectory for the sake of power generation. Then, we introduce a real-time optimization algorithm aimed to improve and adapt the flown path using only the measurements of the wing's position relative to the ground and of the traction forces, i.e. no knowledge of the wind direction or profile. We present the results obtained by applying the approach in numerical simulations.

## II. System description and problem formulation

We consider an AWE generator that exploits aerodynamic lift to produce electrical energy. For an overview see e.g. [1]. The main components of the generator are the ground unit, the tether, and the wing. The tether is used to anchor the wing to the ground unit, where realizations with one or multiple tethers are possible. The wing is flown on a periodic path, sustained by the aerodynamic lift, which results in a traction force $F$ on the tether. The electricity is either generated on-board of the wing, with small propellers and on-board generators [3], or in the ground unit, by unreeling the tether from drums connected to generators [5], [6], [7], [9].

We define a right-handed inertial coordinate system $(\mathbf{e}_x, \mathbf{e}_y, \mathbf{e}_z)$, fixed to the ground unit (see Fig. 1). The unit vectors $\mathbf{e}_x$ and $\mathbf{e}_y$ are parallel to the ground and $\mathbf{e}_z$ is vertical to the ground pointing upwards. The wing's position $p$ can be described by spherical coordinates consisting of the two angles $\varphi$ and $\vartheta$ and the tether length $r$. Assuming a straight tether, the azimuthal angle $\varphi$ defines the angle between the projection of the tether on the ground and the $\mathbf{e}_x$ axis and the elevation $\vartheta$ represents the angle between the tether and the ground plane $(\mathbf{e}_x, \mathbf{e}_y)$. We assume that the incoming wind is parallel to the ground and its misalignment with respect to $\mathbf{e}_x$ is denoted by $\varphi_W$, see Fig. 1.

Due to boundary layer flow effects of the wind above the earth's surface, the magnitude of the wind $W$ is a function of the altitude $z$ above the ground, the so-called wind shear effect. Common choices to model such a wind shear are the log or the power laws [19]. In this paper, we consider the latter, but the results hold for a general monotonically increasing wind profile. In our coordinate system, the altitude is given by $z = r\sin\vartheta$ and the power law is defined as

A. Zgraggen, L. Fagiano, and M. Morari are with Automatic Control Laboratory, Swiss Federal Institute of Technology, Switzerland zgraggen|fagiano|morari@control.ee.ethz.ch

This research has received funding from the California Energy Commission under the EISG grant n. 56983A/10-15 "Autonomous flexible wings for high-altitude wind energy generation", from the European Union Seventh Framework Programme (FP7/2007-2013) under grant agreement n. PIOF-GA-2009-252284 - Marie Curie project "Innovative Control, Identification and Estimation Methodologies for Sustainable Energy Technologies", and from the Swiss Competence Center Energy and Mobility (CCEM).

* Corresponding author: zgraggen@control.ee.ethz.ch.

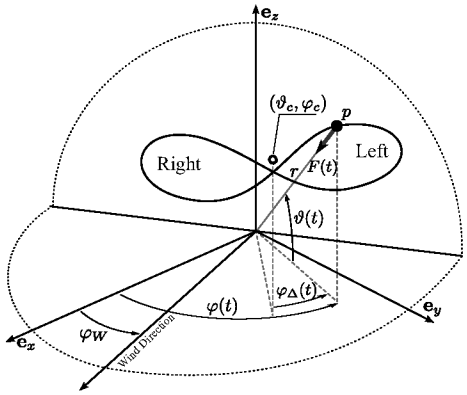


Fig. 1. The wing's position $p = (\varphi(t), \vartheta(t), r(t))$ (black dot) is shown on a figure eight path. The average location of the path (circle) is denoted by $(\varphi_c, \vartheta_c)$. The prevalent wind direction forms an angle $\varphi_W$ with the fixed axis $\mathbf{e}_x$. The wind window is depicted with dotted lines.

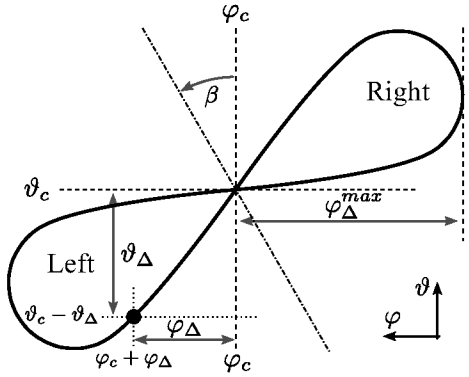


Fig. 2. A general inclined path with average position $(\varphi_c, \vartheta_c)$. The $(\varphi, \vartheta)$ coordinates are depicted as seen from the ground unit and looking at the wing. A point on the path is shown as a black dot. The angle $\beta$ defines the inclination of the path, whose symmetry line is shown as dash-dotted line.

$$W(\vartheta) = W_0 \left( \frac{r \sin \vartheta}{Z_0} \right)^{\alpha}, \tag{1}$$

where $W_0$ is the reference wind speed at the reference altitude $Z_0$ and $\alpha$ is the power law exponent, which depends on the roughness of the surface [19].

In AWE systems, during power generation the tethered wing cannot fly upwind, surpassing its anchor point against the wind. Thus, its motion is restricted on a quarter sphere, called "wind window", defined by the tether length $r$, the ground plane $(\mathbf{e}_x, \mathbf{e}_y)$, and a vertical plane perpendicular to the prevalent direction of the wind field and containing the anchor point of the tether (see Fig. 1, dotted lines). The wing is assumed to fly periodic paths in the wind window, under the action of a feedback controller $K$. Such a path can be described by a set of points in the $(\varphi, \vartheta)$-plane. The average position of the path is denoted by $(\varphi_c, \vartheta_c)$. The angular distances of each point on the path from such an average position are denoted by $\varphi_\Delta$ and $\vartheta_\Delta$, respectively. By introducing the continuous time variable $t$, we can define the corresponding trajectory as the pair

$$\varphi(t) = \varphi_c + \varphi_\Delta(t), \qquad \vartheta(t) = \vartheta_c + \vartheta_\Delta(t)$$

with the trajectory period $T$, i.e.

$$\varphi_\Delta(t+T) = \varphi_\Delta(t), \qquad \vartheta_\Delta(t+T) = \vartheta_\Delta(t).$$

We define the left and right half paths as the points where $\varphi_\Delta(t) \geq 0$ and $\varphi_\Delta(t) < 0$, respectively.

For systems with multiple tethers, the path has to be such that they do not coil up during one period and therefore we will consider paths shaped like an eight, see e.g. [11]. We assume that the path is symmetric in the $(\varphi, \vartheta)$-plane w.r.t. a line, drawing an angle $\beta$ ("inclination") with the line $\varphi = \varphi_c$. The range of $\varphi_\Delta$ values is given by $\varphi_\Delta(t) \in [-\varphi_\Delta^{max}, \varphi_\Delta^{max}]$ with $\varphi_\Delta^{max} > 0$. The maximal $\varphi_\Delta(t)$ value, $\varphi_\Delta^{max}$, defines the span of the path, since it accounts for half of the total span. See Fig. 1-2 for a graphical representation.

The dynamics of this system can be generally described as

$$\begin{aligned} \dot{x} &= f(x, u, \varphi_W, W_0, Z_0, \alpha) \\ y &= g(x, u), \end{aligned} \tag{2}$$

where $x$ denotes the states, $u$ the control input, and $y$ the measured output. The wind cannot be easily measured or estimated, hence we assume that the wind direction $\varphi_W$ and parameters $W_0$, $Z_0$, $\alpha$ are not precisely known. The control input $u$ is computed by the controller $K$, which is a discrete system with internal state $z$, input $y$, and parameters $\Theta$.

$$K : \begin{cases} z(\tau+1) &= h_z(z(\tau), y(\tau), \Theta(\tau)) \\ u(t) &= h_u(z(\tau), y(\tau), \Theta(\tau)), \quad t \in [\tau T_s, (\tau+1) T_s) \end{cases} \tag{3}$$

where $\tau \in \mathbb{N}$ is the discrete sampling instant with sampling time $T_s$. The parameters $\Theta$ contain specifications of the wing's path, namely the average position of the path $(\varphi_c, \vartheta_c)$, its span $\varphi_\Delta^{max}$ and inclination $\beta$, and it is assumed that the controller $K$ is able to attain such specifications.

We consider a constant reel-out speed, thus the maximization of the average force $\bar{F}$ implies a maximization of the average power produced during the cycle:

$$\bar{F} = \frac{1}{T} \int_0^T F(t) dt. \tag{4}$$

In the considered settings, $\bar{F}$ is a function of the controller's parameters $\Theta$, i.e. our decision variables, and of the wind field, described here by its direction $\varphi_W$ and wind shear parameters $W_0$, $Z_0$, $\alpha$, which are uncertain. Our aim is to find the parameters $\Theta$ such that the average traction force (hence the average power) is maximal. The related optimization problem can be formulated as

$$\max_{\Theta} \qquad \bar{F}(\Theta, \varphi_W, W_0, Z_0, \alpha). \tag{5}$$

The exact solution of (5) would require the precise knowledge of the wind profile and direction, which are not assumed to be available here. In order to tackle this problem, we proceed in two steps. First, we analyze the influence of $\Theta$ on the average traction force; then, we propose a general algorithm, to be used on top of controller $K$, able to solve

(5) by dealing with the uncertainty of the wind direction and profile.

## III. Crosswind traction force

We first investigate the properties of the average traction force for a flown path using a simplified model, which allows an analytical study of the force as a function of the parameters $\Theta$.

### A. Analysis of the traction force with a simplified model

A simplified model to estimate the traction force of a tethered wing depending on its location has been introduced in [2] and subsequently refined in several contributions, see e.g. [2], [20]. According to this model, for a constant reeling speed, the traction force $F$ is a function of the current location of the wing and of the wind:

$$F(\varphi, \vartheta, \varphi_W, W_0, Z_0, \alpha) = \mathcal{C}\, v(\vartheta)\, m(\varphi - \varphi_W), \tag{6}$$

where

$$\mathcal{C} = \frac{1}{2}\rho A C_L E_{eq}^2 \left(1 + \frac{1}{E_{eq}^2}\right)^{\frac{3}{2}} \tag{7}$$
$$v(\vartheta) = W(\vartheta)^2 \cos(\vartheta)^2$$
$$m(\varphi - \varphi_W) = \cos(\varphi - \varphi_W)^2$$

and

$$E_{eq} = \frac{C_L}{C_{D,eq}} = \frac{C_L}{C_D + \frac{C_{D,l} A_l}{4A}}. \tag{8}$$

In (7)-(8), the air density is indicated by $\rho$, $A$ is the wing reference area, $C_L$ is the wing's lift coefficient, $C_{D,eq}$ is the equivalent drag coefficient, accounting for the drag of the wing and the added drag by the cable. $C_{D,l}$ is the drag coefficient of the cable and $A_l = n_l\, r\, d_l$ is the cable reference area, where $n_l$ is the number of lines supporting the wing, $r$ is the line length, and $d_l$ is the line diameter. For simplicity, the values of $C_L$ and $C_D$ are assumed to be constant, as considered e.g. in [10].

Equations (6)-(8) allow an analysis of the traction force as a function of the parameters $\Theta$. Since the wing is assumed to fly within the wind window, we limit the analysis to the following ranges:

$$\begin{aligned} \varphi_c &\in (\varphi_W - \pi/2, \varphi_W + \pi/2) \\ \vartheta_c &\in (0, \pi/2) \\ \varphi_\Delta^{max} &\in (0, \pi/2 - (\varphi_c - \varphi_W)] \\ \beta &\in [-\pi/2, \pi/2]. \end{aligned}$$

By inspection, function $m(\varphi_c - \varphi_W) : (\varphi_W - \pi/2, \varphi_W + \pi/2) \mapsto (0, 1]$ is a quasi-concave function with its maximum at $\varphi = \varphi_W$. Function $v(\vartheta_c) : (0, \pi/2) \mapsto \mathbb{R}_+$ consists of two parts. The first part, the wind profile $W(\vartheta)$, is assumed to be monotonically increasing, according to (1), and the second part, $\cos(\vartheta)^2$, is also a quasi-concave function in the domain of $v$. By using the second-order condition for quasi-concave functions [21], it can be verified that the product is still quasi-concave and that the point $(\varphi, \vartheta)$ in the wind window with maximal traction force for (6) is given by $(\varphi_W, \arctan(\sqrt{\alpha}))$.

We will now compute the average traction force for a given path using (6). By introducing the index $k = 1, \ldots, N$, which identifies the samples of a discretized path with sampling time $T_s$, any sampled position in the path can be expressed as $(\varphi_c + \varphi_\Delta(k), \vartheta_c + \vartheta_\Delta(k))$. The discrete form of the average traction force (4) can be then written as

$$\frac{1}{T}\int_0^T F(t)dt \simeq \frac{1}{NT_s}\sum_{k=1}^{N} F(k)T_s = \frac{1}{N}\sum_{k=1}^{N} F(k) \tag{9}$$

The average traction force $\bar{F}$ for one period of the path is thus given by

$$\bar{F}(\Theta, \varphi_W, W_0, Z_0, \alpha) = \frac{1}{N}\sum_{k=1}^{N} \mathcal{C}\, v(\vartheta(k))\, m(\varphi(k) - \varphi_W), \tag{10}$$
$$\text{with} \quad \begin{aligned} \vartheta(k) &= \vartheta_c + \vartheta_\Delta(k) \\ \varphi(k) &= \varphi_c + \varphi_\Delta(k) \end{aligned}$$

For the following analysis, we focus on the dependence of $\bar{F}$ on $\varphi_c$, $\vartheta_c$, and $\varphi_\Delta^{max}$ only, and fix the inclination $\beta = 0$ (see Fig. 2). In Fig. 3, the average traction force (10) as a function of $\varphi_c - \varphi_W$ for different $\vartheta_c$ is shown. Note that the forces in all the plots have been normalized in order to emphasize the independence of the qualitative behavior on the wind: stronger winds influence only the numerical values, but the qualitative behavior of the average force remains unchanged.

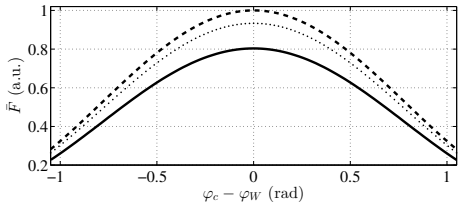


Fig. 3. Average traction force computed with the simplified model with $\varphi_\Delta^{max} = 0.3$. Solid: $\vartheta_c = 0.1$, dashed: $\vartheta_c = 0.3$, and dotted: $\vartheta_c = 0.5$.

From (10), we can notice that the contributions of the left and right half paths to the average traction force $\bar{F}$ are not the same if $\varphi_c \neq \varphi_W$. We therefore derive the average traction forces for each of the half paths, and investigate the influence of the parameters $\Theta$ on their difference. The average traction forces of the left and right half paths are:

$$\begin{aligned} \bar{F}_L &= \frac{1}{N_L}\sum_{k=1}^{N_L} \{\mathcal{C} v(\vartheta(k)) m(\varphi(k) - \varphi_W) | \varphi(k) \geq \varphi_c\} \\ \bar{F}_R &= \frac{1}{N_R}\sum_{k=1}^{N_R} \{\mathcal{C} v(\vartheta(k)) m(\varphi(k) - \varphi_W) | \varphi(k) < \varphi_c\}, \end{aligned} \tag{11}$$

where $\bar{F}_L$ and $\bar{F}_R$ stand for the average traction force of the left and right half and $N_L$ and $N_R$ are the corresponding number of samples.

The traction force difference between the left and right halves, using (7) and (11), is given, after some manipulations and assuming a sufficiently small sampling time, by

$$\begin{aligned} \Delta\bar{F}(\Theta, \varphi_W, W_0, Z_0, \alpha) &= \bar{F}_L - \bar{F}_R \\ &\simeq \frac{\mathcal{C}}{2}\sin(2(\varphi_W - \varphi_c))\mathcal{B}, \end{aligned} \tag{12}$$

where the positive term $\mathcal{B}$ is given by

$$\mathcal{B} = \frac{1}{N_L}\sum_{k=1}^{N_L} v(\vartheta(k))\sin(2|\varphi_\Delta(k)|) + \frac{1}{N_R}\sum_{k=1}^{N_R} v(\vartheta(k))\sin(2|\varphi_\Delta(k)|)$$

From (12) it can be seen that the difference in traction force is zero only if $\varphi_c = \varphi_W$ and that it is monotonic for $|\varphi_c - \varphi_W| \leq \pi/4$. Moreover, paths with an average position on the left of the wind direction, as seen from the anchor point of the tether (i.e. $\varphi_c - \varphi_W > 0$), have a negative $\Delta\bar{F}$, and vice-versa (see Fig. 4). This is due to the smaller fraction of the incoming wind being in tether direction, thus generationg less traction force. In Fig. 4, a plot of $\Delta\bar{F}$ for different values of the half-span $\varphi_\Delta^{max}$ is shown. By changing the span of the path, the magnitude of $\Delta\bar{F}$ changes. For larger spans, the difference between the average traction force given by the left and right half paths gets larger. The span of the path also has an influence on the average traction force, see Fig. 5, i.e. wider paths provide smaller average traction force. Thus, a path which has a higher traction force due to its small span will also have a smaller magnitude in $\Delta\bar{F}$. By changing the elevation of the path, $\vartheta_c$, the values of $\bar{F}$ and $|\Delta\bar{F}|$ change according to the value of $v(\vartheta)$ from (7). This is shown in Fig. 3 for $\bar{F}$. In particular, there is a single value of $\vartheta_c$ that maximizes the traction force, and this value depends only on the wind profile and not on the misalignment $(\varphi_W - \varphi_c)$.

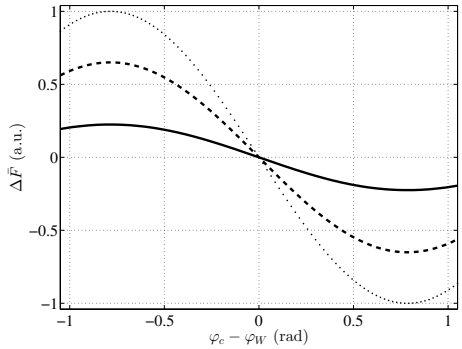


Fig. 4. Difference of average traction forces $\Delta\bar{F}$ computed with the simplified model, with $\vartheta_c = 0.2$ and different values of the span. Solid: $\varphi_\Delta^{max} = 0.1$, dashed: $\varphi_\Delta^{max} = 0.3$, and dotted: $\varphi_\Delta^{max} = 0.5$.

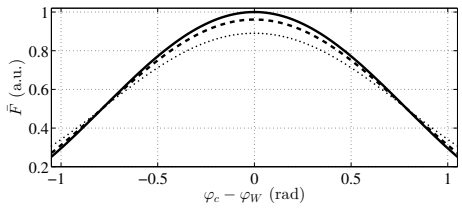


Fig. 5. Average traction force computed with the simplified model, with $\vartheta_c = 0.2$ and different values of the span. Solid: $\varphi_\Delta^{max} = 0.1$, dashed: $\varphi_\Delta^{max} = 0.3$,and dotted: $\varphi_\Delta^{max} = 0.5$.

### *B. Analysis of the traction force with a dynamic model*

In this section, we employ a dynamic model to asses the considerations derived in section III-A, and to analyze the effects of different path inclinations $\beta$ on the average forces. The dynamics $f(x,u,\varphi_W,W_0,Z_0,\alpha)$ are modeled here by a widely used nonlinear point-mass model for a tethered wing, see e.g. [10], [11], [12], [16], [22], [23]. The dynamic equations are derived from first principles and the wing is assumed to be a point-mass. The tether is assumed to be straight with a distributed mass and non-zero diameter. The aerodynamic drag of the tether and half of the tether mass are added to the wing's drag and mass, respectively. The aerodynamic forces are modeled with constant lift and drag coefficients, and effects from gravity and inertial forces are included. Defining the transversal axis of the wing to point from the left wing tip to the right wing tip, we can describe the roll angle $\psi$ as the angle which is drawn between the transversal axis and the tangent plane on the wind window at the wing's position. The wing is assumed to be steered by a non-zero roll angle, which is manipulated by a control system, and thus, referring to (2), we have $u = \psi$. The state $x$ of this system is given by $x = (\varphi, \vartheta, r, \dot{\varphi}, \dot{\vartheta}, \dot{r})$.

In order to carry out the simulations, the controller $K$ is designed using the approach described in [24]. Such a controller is able to obtain a symmetric figure eight path with a required span and inclination, and with the average position being a given reference location $(\varphi_c, \vartheta_c)$.

Consistently with Section III-A, the average traction forces generated during the full path, and the average traction force generated on the left and right half paths, are computed from the simulation results:

$$\bar{F}(\Theta,\varphi_W,W_0,Z_0,\alpha) = \frac{1}{N}\sum_{k=1}^{N} F(k)$$

$$\bar{F}_L = \frac{1}{N_L}\sum_{k=1}^{N_L}\{F(k)\,|\varphi(k) \geq \varphi_c\}$$

$$\bar{F}_R = \frac{1}{N_R}\sum_{k=1}^{N_R}\{F(k)\,|\varphi(k) < \varphi_c\}\,.$$

The traction force difference between the left and right half path is

$$\Delta\bar{F}(\Theta,\varphi_W,W_0,Z_0,\alpha) = \bar{F}_L - \bar{F}_R\,.$$

As done before, we want to know how $\bar{F}$ and $\Delta\bar{F}$ change for different values of $\Theta$, including the inclination $\beta$.

Comparing the traction force for various $\varphi_c$ and $\vartheta_c$ with a symmetric horizontal path shape (i.e. $\beta = 0$) shows good qualitative correspondence with the simplified model used in Section III-A, thus indicating that gravity and inertial forces do not change the system behavior. If the path is inclined, i.e. $\beta \neq 0$, the average traction force does not increase more than 2% for $\varphi_c$ around the optimum of $\bar{F}$, but the values of $\Delta\bar{F}$ change significantly. In fact, when the path is inclined, the traction force difference is not zero anymore for $\varphi_c - \varphi_W = 0$, see Fig. 6. The effect of larger spans in the presence of $\beta \neq 0$ is the same as the one observed in Section III-A, i.e. a larger value of $\varphi_\Delta^{max}$ increases $\Delta\bar{F}$ for fixed values of the other parameters. As expected from the simplified analysis, stronger wind or different tether length $r$ do not affect the qualitative results.

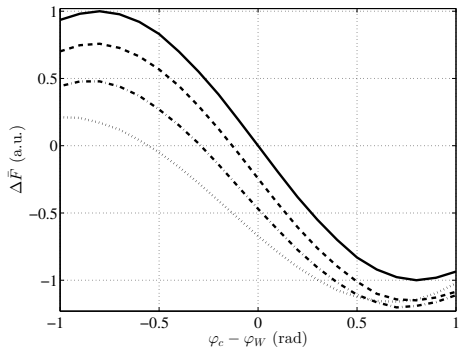


Fig. 6. Traction force difference $\Delta\bar{F}$ computed with the point-mass model for $\vartheta_c = 0.4$, $\varphi_\Delta^{max} = 0.24$, and different inclinations $\beta = 0$ (solid), $\beta = 0.3$ (dashed), $\beta = 0.6$ (dot-dashed), and $\beta = 0.9$ (dotted).

### C. Discussion

The results of the previous two sections show that there is a single optimal average location, denoted as $(\varphi_c^*, \vartheta_c^*)$, yielding the maximal average traction force for a given path shape. In particular, we have $\varphi_c^* = \varphi_W$, while $\vartheta_c^*$ depends on the vertical wind profile. The average traction force is very sensitive on the average position of the path. A misalignment in $\varphi_c$ with respect to $\varphi_c^*$ of roughly 20° can lead to a decrease of average traction force of 15%, while 50% of the force is obtained for a misalignment of roughly 45°, see Fig. 3. An average elevation $\vartheta_c \neq \vartheta_c^*$ can also reduce the traction force by a significant amount, in the same order as for $\varphi_c$.

The difference in average traction force, $\Delta\bar{F}$, is zero for horizontal paths with an average position $\varphi_c = \varphi_W$. Moreover, for paths with zero inclination, the sign of $\Delta\bar{F}$ is the opposite w.r.t. that of $\varphi_c - \varphi_W$, i.e. $\varphi_c - \varphi_c^*$. Therefore, the value of $\Delta\bar{F}$ is a good indicator of the alignment of $\varphi_c$ with the wind direction $\varphi_W$. However, $\Delta\bar{F}$ is sensitive to changes in $\beta$. With $\beta \neq 0$ the difference in traction force $\Delta\bar{F}$ is not anymore zero for $\varphi_c = \varphi_W$, and the sign of $\Delta\bar{F}$ is not the opposite w.r.t the sign of the misalignment $\varphi_c - \varphi_W$ anymore (see Fig. 6).

The span of the path in the elevation direction $\vartheta$ was not considered in this work. However, from our analysis the effects of this aspect on the average traction force are similar to the one seen for the lateral span $\varphi_\Delta^{max}$.

In conclusion, the analysis above shows that optimizing the average position $(\varphi_c, \vartheta_c)$ yields the largest increase of average traction force (hence generated power). The shape of the path, in terms of span and inclination, has only a relatively small influence on the traction force. In the next section, we exploit these considerations to derive an algorithm able to optimize in real-time the average path location, using only the measurements of traction force on the tethers.

## IV. Real-time optimization and adaptation algorithm

As seen in the previous section, the average location of a flown path has the largest influence on the generated traction force among all of the considered parameters. Thus we aim to find the best average location in $\varphi$ and $\vartheta$ for a given path shape, in order to maximize the average power output of the AWE system. Since the inclination of a path has an adverse effect on $\Delta\bar{F}$ and does not affect $\bar{F}$, we only consider horizontal paths with $\beta = 0$. Enforcing a horizontal path can be done in practice with a suitable controller as in [25]. Thus, in the following we consider $\Theta \doteq (\varphi_c, \vartheta_c)$ as optimization variables, fix the half-span $\varphi_\Delta^{max}$ to a prescribed value and select $\beta = 0$.

Recall that we assume that the underlying controller accepts reference values for the average location where the path should be flown. The presented algorithm will then compute such reference values in order to solve the following optimization problem:

$$\max_{\varphi_c, \vartheta_c} \quad \bar{F}(\Theta, \varphi_W, W_0, Z_0, \alpha)\,. \tag{13}$$

We assume that the parameters $\varphi_W, W_0, Z_0, \alpha$, specifying the wind direction and profile, are not known, hence the optimization problem (13) is uncertain due to the lack of information on $\varphi_W$ and the wind shear profile. On the other hand, we assume that the traction force $F$ is measured, as well as the position of the wing w.r.t. the ground unit. Hence the values of $\bar{F}$ and $\Delta\bar{F}$ for each flown path are measured.

The analysis presented in the previous section indicates that we can reformulate the optimization problem as

$$\max_{\vartheta_c} \left[ \max_{\varphi_c} \quad \bar{F}(\Theta, \varphi_W, W_0, Z_0, \alpha) \right], \tag{14}$$

i.e. (14) can be maximized separately in $\varphi_c$ and $\vartheta_c$. Also, note that for horizontal paths we have

$$\arg\max_{\varphi_c} \bar{F}(\Theta, \varphi_W, W_0, Z_0, \alpha) = \arg\min_{\varphi_c} |\Delta\bar{F}(\Theta, \varphi_W, W_0, Z_0, \alpha)| \tag{15}$$

as it can be derived from (10) and (12) and from the results in Section III-B. Therefore, the problem (13) can be solved by addressing two subsequent optimization problems independently. We will first exploit the measure of $\Delta\bar{F}$ to find the best location in $\varphi$, i.e. to compute $\arg\min |\Delta\bar{F}(\Theta, \varphi_W, W_0, Z_0, \alpha)|$, and then the measure of $\bar{F}$ to find the best location in $\vartheta$, i.e. solving (14) with the previously found optimal $\varphi_c$. The advantage of using $\Delta\bar{F}$ to find the optimal $\varphi_c$, instead of using only $\bar{F}$, is that a single value of $\Delta\bar{F}$, i.e. a single flown path, gives a qualitative indication of the misalignment $\varphi_c - \varphi_W$. By using only $\bar{F}$, the values obtained by two paths, with different $\varphi_c$, would be needed to estimate the search direction for the parameter $\varphi_c$, which would take at least twice as long. Thus, the adaptation in $\varphi$ direction is sped up by looking at the traction force difference $\Delta\bar{F}$.

### A. Algorithm Outline

We present a short outline of an algorithm which is able to adapt the average position of a path, such that it converges to the optimum. The algorithm iterates over subsequent complete paths flown by the wing, and exploits the values of $\bar{F}$ and $\Delta\bar{F}$ measured in the current and past paths. It uses a coordinate search approach, see e.g. [26], to solve the two subsequent optimization problems, since no gradient information is available. The value $\Delta\bar{F}_{min}$ is used as a stopping criterion for the $\varphi$ direction adaptation.

**Algorithm 1:** Optimization/Adaptation

```
while true do
    if |ΔF̄| > ΔF̄_min then
        min_{φ_c} |ΔF̄|
        update φ_c
    else
        max_{ϑ_c} F̄
        update ϑ_c
    end
end
```

TABLE I
POINT-MASS MODEL PARAMETERS

| | | | | | | | | |
|---|---|---|---|---|---|---|---|---|
| $A$ | = | 9 m | $m$ | = | 2.45 kg | $r$ | = | 30 m |
| $n_l$ | = | 3 | $d_l$ | = | 0.003 m | | | |
| $C_L$ | = | 0.8 | $C_D$ | = | 0.134 | $C_{D,l}$ | = | 1.2 |
| $W_0$ | = | 5 m/s | $Z_0$ | = | 4 m | $\alpha$ | = | 0.1 |

## V. NUMERICAL SIMULATIONS

We tested the approach in simulation using the same point-mass dynamical model of the system as in [12] and the controller presented in [25]. The results indicate that the approach is able to tune in real-time the controller in order to follow a changing wind direction and adapt the paths' average elevation according to the (unknown) wind profile. The main parameters of the model are listed in Tab. I. A plot with the time course of the average location of the path and the wind direction can be seen in Fig. 7.

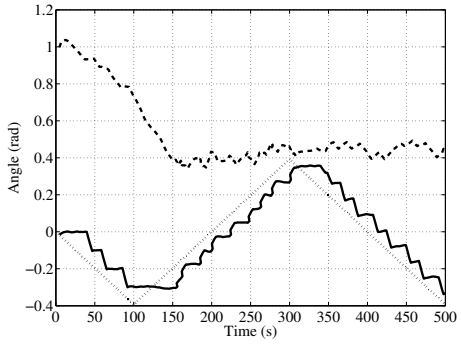


Fig. 7. Simulation results obtained by applying the proposed algorithm on the point-mass model. The solid and dashed lines represent the average $\varphi$ and $\vartheta$ positions of the path, $\varphi_c$ and $\vartheta_c$, respectively. The dotted line shows the wind direction.

## VI. CONCLUSION AN FUTURE WORK

We presented an analysis of the average traction force generated by a tethered wing and, based on the results of such analysis, we proposed an algorithm to adapt and optimize in real-time the average position of the flown path without exact knowledge of the wind direction and profile. The algorithm is not dependent on the system configuration, e.g. number of lines or position of the generator, and it can be used as an extension of any working controller for a tethered wing, provided that the controller is able to fly the wing on a symmetric horizontal path and to attain a reference position in terms of average location of the path in the wind window. We tested the approach with numerical simulations, showing a good performance in adapting and optimizing the system's operation in the presence of unknown and changing wind conditions. Real-world experiments on a small-scale prototype have been carried out as well (see [27]) and the results will be presented in the near future.

## REFERENCES


[1] L. Fagiano and M. Milanese, "Airborne wind energy: an overview," in *American Control Conference 2012*, Montreal, Canada, 2012, pp. 3132–3143.

[2] M. L. Loyd, "Crosswind kite power," *Journal of Energy*, vol. 4, pp. 106–111, June 1980.

[3] Makani Power Inc., http://www.makanipower.com.

[4] Skysails Power GmbH, skysails Power website, http://www.skysails.info/english/power/.

[5] Ampyx power website, http://www.ampyxpower.com/.

[6] Windlift, Inc., windlift website, http://www.windlift.com/.

[7] Kitenergy Srl, kitenergy website, http://www.kitenergy.net/.

[8] Enerkite GmbH, enerkite website, http://www.enerkite.de/.

[9] Swiss Kite Power website, http://www.swisskitepower.ch/.

[10] M. Canale, L. Fagiano, and M. Milanese, "Power kites for wind energy generation," *IEEE Control Systems Magazine*, vol. 27, no. 6, pp. 25–38, December 2007.

[11] A. Ilzhöfer, B. Houska, and M. Diehl, "Nonlinear MPC of kites under varying wind conditions for a new class of large-scale wind power generators," *International Journal of Robust and Nonlinear Control*, vol. 17, pp. 1590–1599, 2007.

[12] M. Canale, L. Fagiano, and M. Milanese, "High altitude wind energy generation using controlled power kites," *IEEE Transactions on Control Systems Technology*, vol. 18, no. 2, pp. 279 –293, mar. 2010.

[13] E. Terink, J. Breukels, R. Schmehl, and W. Ockels, "Flight dynamics and stability of a tethered inflatable kiteplane," *AIAA Journal of Aircraft*, vol. 48, no. 2, pp. 503–513, 2011.

[14] C. Vermillion, T. Grunnagle, and I. Kolmanovsky, "Modeling and control design for a prototype lighter-than-air wind energy system," in *American Control Conference (ACC)*, 2012, pp. 5813–5818.

[15] J. H. Baayen and W. J. Ockels, "Tracking control with adaption of kites," *IET Control Theory and Applications*, vol. 6, no. 2, pp. 182–191, 2012.

[16] P. Williams, B. Lansdorp, and W. Ockels, "Optimal crosswind towing and power generation with tethered kites," *Journal of guidance, control, and dynamics*, vol. 31, pp. 81–93, 2008.

[17] B. Houska and M. Diehl, "Optimal control for power generating kites," in *European Control Conference (ECC), Kos, Greece, 2.-5. July*, 2007.

[18] S. Costello, G. Franois, and D. Bonvin, "Real-time optimization for kites," in *Proceedings of the IFAC Workshop on Periodic Control Systems, Caen, France, 3.-5. July*, 2013, pp. 64–69.

[19] M. L. Ray *et al.*, "Analysis of wind shear models and trends in different terrains," in *AWEA Proceedings of AWEA Windpower 2006 Conference, 4.-7. June*, Pittsburgh, PA, 2006.

[20] L. Fagiano, M. Milanese, and D. Piga, "Optimization of airborne wind energy generators," *International Journal of Robust and Nonlinear Control*, vol. 22, no. 18, pp. 2055–2083, 2012.

[21] S. Boyd and L. Vandenberghe, *Convex Optimization*. Cambridge University Press, 2004.

[22] M. M. Diehl, "Real-time optimization for large scale processes," Ph.D. dissertation, Ruprecht-Karls-Universität Heidelberg, June 2001.

[23] L. Fagiano, "Control of tethered airfoils of high-altitude wind energy generation," Ph.D. dissertation, Politecnico di Torino, 2009.

[24] L. Fagiano, A. Zgraggen, and M. Morari, "On modeling, filtering and automatic control of flexible tethered wings for airborne wind energy," in *Airborne Wind Energy*. Springer, 2013, pp. 167–180.

[25] L. Fagiano, A. Zgraggen, M. Morari, and M. Khammash, "Automatic crosswind flight of tethered wings for airborne wind energy: modeling, control design and experimental results," *IEEE Transactions on Control Systems Technology*, 2013, in press.

[26] A. R. Conn, K. Scheinberg, and L. N. Vicente, *Introduction to Derivative-Free Optimization*. Philadelphia, PA, USA: Society for Industrial and Applied Mathematics, 2009.

[27] EISG project "Autonomous flexible wings for high-altitude wind energy generation", experimental test movie, October 2012. Available on–line: http://youtu.be/5prsTSiLFIw.